HAL
open science

Growth Progression of Oxygenic Photogranules and Its Impact on Bioactivity for Aeration-Free Wastewater Treatment

Ahmed S. Abouhend, Kim Milferstedt, Jérôme Hamelin, Abeera A. Ansari, Caitlyn Butler, Blanca I. Carbajal-Gonzalez, Chul Park

▶ **To cite this version:**

HAL Id: hal-02629305
https://hal.inrae.fr/hal-02629305v1

Submitted on 6 Jul 2023

Progression in photogranules and its effect on oxygenic function for aeration-free wastewater treatment

Ahmed S. Abouhend,[†] Kim Milferstedt,[‡] Jérôme Hamelin,[‡] Abeera A. Ansari,[†] Caitlyn Butler,[†] Blanca I. Carbajal-González,[§] Chul Park[*,†]

[†]Department of Civil and Environmental Engineering, University of Massachusetts Amherst, Amherst, Massachusetts 01003, United States
[‡]LBE, Univ Montpellier, INRA, Narbonne F-11100, France
[§]Science Center Microscopy Facility, Mount Holyoke College, South Hadley, Massachusetts 01075, United States
[1]Corresponding author: chulp@umass.edu

ABSTRACT: Oxygenic photogranules (OPGs), spherical aggregates comprised of phototrophic and non-phototrophic microorganisms, treat wastewater without aeration, which currently incurs the highest energy demand in wastewater treatment. In wastewater-treating reactors, photogranules grow in number as well as in size. Currently, it is unknown how the photogranules grow in size and how this growth impacts their properties and performance in wastewater treatment. Here, we present that the photogranules' growth occurs with changes in phototrophic community and granular morphology. We observed that as the photogranules grow in size, filamentous cyanobacteria become enriched while other phototrophic microbes diminish significantly. The photogranules greater than approximately 3 mm in diameter showed the development of a layered structure in which a concentric filamentous cyanobacterial layer encloses non-cyanobacterial aggregates. The diameter of the non-cyanobacterial core increased linearly with the photogranule's size. The depth of the outer cyanobacterial layer, however, remained unchanged, suggesting the boundary conditions for cyanobacterial growth to occur within photogranules. We observed that the growth of photogranules significantly impacts their capability of producing oxygen, the key element in aeration-free wastewater treatment by OPGs. We discuss engineering the OPG process based on photogranules' size, promoting the stability of the granular process and enhancing efficiency for self-aerating wastewater treatment.

TOC/ABSTRACT ART
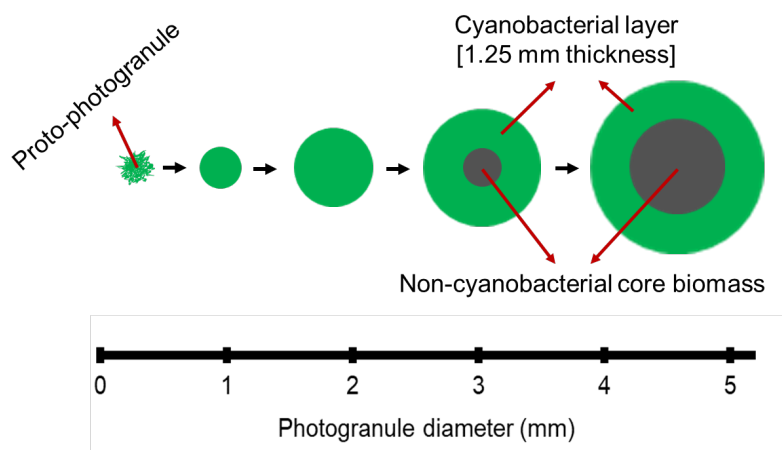
INTRODUCTION

Photogranulation is a light-driven microbial process in which phototrophic microorganisms and non-phototrophic microorganisms form spherical aggregates. This phenomenon seems to occur ubiquitously since its products, i.e., photogranules, are formed in widely varying environments, including lake water,[1] sea water,[2–5] melt holes on glacier surfaces (i.e., cryoconite holes),[6–8] and wastewater treatment systems.[9–18]

Oxygenic photogranules (OPGs) are a new photogranule type that has been recently developed for wastewater treatment applications.[9,10,17,18] In OPGs, oxygenic phototrophs live in close proximity to other microbes that possess the necessary functional traits for wastewater treatment.[10] Hence, OPGs can remove organic matter and nutrients using the oxygen generated through photosynthesis, rather than relying on oxygen provided from energy intensive aeration by mechanical means.[9,10,17,18]

OPGs were first reported from a fortuitous discovery that activated sludge stored in a closed hydrostatic environment with a source of light transforms into a photogranule.[9,10] This "hydrostatic photogranulation" occurs with the enrichment of phototrophic microorganisms, including green algae, diatoms, and filamentous cyanobacteria, which were initially present at extremely low levels in activated sludge.[10] Among these phototrophs, filamentous cyanobacteria, particularly the order *Oscillatoriales*, are considered the key granulating microbial group, because not only they are found at the highest population in formed photogranules but also their mat-like layer maintains the photogranule's structural integrity.[10,19,20] Formed out of activated sludge under hydrostatic conditions, these photogranules have been reported to be 10–20 mm in diameter.[10,19,20]

The application of OPGs for a flow-based wastewater treatment has been demonstrated with stable and successful reproduction of reactor operation.[10,17,18] The OPG process for wastewater treatment starts by seeding a stirred-tank reactor with hydrostatically-formed photogranules and operating in sequencing batch mode under cyclic light conditions.[9,10,17,18] Over the first few days, the seed photogranules disintegrate and new photogranular biomass is produced. As reactor operation continues, the photogranules substantially increase in number as well as in size, resulting in an increase in biomass concentration, simultaneously occurring with the treatment of wastewater. Abouhend *et al.*[17] showed that during the steady-state operation of the OPG process, the size of biomass in reactors was in the range of 0.1–4.5 mm in diameter. While these reactor photogranules are smaller than hydrostatically-formed photogranules and are generated in the presence of shear with input of wastewater, the two photogranule types are very similar by predominance of filamentous cyanobacteria.[10,17] Milferstedt *et al.*[10] also showed that large-size photogranules grown in reactors possessed the layered structure similar to hydrostatically-formed photogranules.

Previous studies on other granular biotechnologies, such as aerobic granular sludge, showed that the structure of granules changes as the granules grow larger.[21–25] Changes in size and structure influence mass transfer in granules, further causing changes in ecology, physiology, as well as physicochemical properties of granules.[21–25] Hence, granule size is directly related with the characteristics and functions of granules and ultimately determines the performance of bioprocesses. Although the growth of photogranules in size is obvious in OPG reactor operation,[10,17,18] the structural as well as community changes along with size progression remain mainly unknown. Moreover, since oxygen is produced within the photogranules, not diffusing from bulk liquid by aeration as occurring in aerobic granule sludge,[24,26,27] the size of the photogranules is expected to impact their oxygen production capability. This key element of the OPG process has remained unexplored until this study.

Here, we present the progression in photogranules growing in reactors and how it impacts the biomass's oxygenic function. The study shows that the increase in the size of photogranules occurs with the change in phototrophic community, especially with the increase in filamentous cyanobacteria. We observed that a distinct cyanobacterial layer develops as the photogranules grow larger than a certain size. The study also reports the changes in the quantity and composition of extracellular polymeric substances (EPS) to illustrate how EPS change along with the photogranule's size evolution. We determined that photogranule size indeed has a major influence on oxygen production. This study is, therefore, expected to help engineer the OPG process by maintaining optimal photogranular biomass in the system and achieve effective wastewater treatment without energy intensive aeration.

MATERIALS AND METHODS

Detailed methods are provided in Supplementary Information.

Source and Size separation of photogranular biomass. Photogranular biomass investigated in this study was collected from laboratory-scale reactors which were seeded with hydrostatically formed photogranules and operated in sequencing batch mode for five months to treat wastewater without aeration.[17] The photogranular biomass was classified based on size according to the wet-sieving method.[28] Briefly, 500 mL of mixed biomass was collected from the reactors and suspended in a glass beaker containing the reactor's effluent to a total volume of 4 L. The biomass in effluent was then passed through certified testing sieves (Gilson, V200CH) with opening diameters of 0.2 mm, 0.5 mm, 1 mm, 1.7 mm, 2.5 mm, 3.5 mm, and 4.5 mm. The following size classes were then obtained: 1) <0.2 mm; 2) 0.2−0.5 mm; 3) 0.5−1 mm; 4) 1−1.7 mm; 5) 1.7−2.5 mm; 6) 2.5−3.5 mm; and 7) 3.5−4.5 mm.

Microscopy. Brightfield, fluorescence, and scanning electron microscopy (SEM) were performed following the procedure presented in Milferstedt et al.[10] SEM samples were dried using the tertiary butanol method.[29]

Measurements of chlorophylls and phycobilin in photogranules. Extraction and quantification of chlorophylls followed Standard Methods 10200H[30]. The methods by Bennett and Bogorad[31] and Islam et al.[32] were modified and used to determine phycobilin in photogranules. Briefly, three 10 mL photogranular biomass samples were pipetted into centrifuge tubes and centrifuged at 12,000 rpm for 10 min. The biomass pellet was resuspended in 0.025 M phosphate buffer saline (PBS) solution (pH 7) to a volume of 10 mL. The samples in PBS solution were then homogenized, sonicated, and centrifuged. The absorbance of supernatant was measured at the wavelengths 562 nm, 615 nm, and 652 nm. The equations by Bennett and Bogorad[31] were used to quantify the phycocyanin (PC), phycoerythrin (PE) and allophycocyanin (APC). Total phycobilin concentration (mg/mL) in samples was calculated as the sum of PC, PE, and APC concentrations.

Extracellular polymeric substances (EPS) in photogranules. EPS was extracted from the photogranule biomass following the sequential sonication and base extraction method presented in Ansari et al.[18] Polysaccharide and protein concentrations in extracted EPS were measured using the Dubois method[33] and the modified Lowry method,[34] respectively.

Specific oxygen production rate (SOPR) of photogranules. The oxygen production rate (mg O_2/L-h) of each photogranule size class was determined in a closed batch system following the procedure shown in Abouhend et al.[17] Briefly, each photogranule size class was suspended in 2x diluted primary-effluent wastewater and then transferred to a 300 mL biochemical oxygen demand (BOD) bottle with no headspace. The BOD bottles were purged with nitrogen, mixed at 100 rpm using a magnetic stirrer, and then exposed to light at photosynthetically active radiation (PAR) of approximately 150 μmol/m²-s. The

dissolved oxygen concentration in BOD bottles was monitored over time until dissolved O_2 gets saturated. We plotted the dissolved oxygen concentration versus time and then determined "the net oxygen production rate (OPR_{net})" of photogranular biomass as the slope of the linear-regression line.

We also measured the initial and final concentrations of chemical oxygen demand (COD) and nitrogen species in the liquid phase. Next, we calculated the theoretical amount of oxygen consumed ($OPR_{consumed}$) for the oxidation of organic matter and nitrification during the batch reaction. The total OPR (OPR_{total}) of the OPG biomass was obtained by taking the sum of OPR_{net} and $OPR_{consumed}$. The specific OPR (SOPR) of the OPG biomass (mg O_2/g VSS-h) was obtained by dividing OPR_{total} of each size class by the concentration of VSS of photogranular biomass used in the batch experiments.

Analytical methods. Measurements of suspended solids of the photogranular biomass were conducted according to Standard Methods 2540D/E.[30] Zone settling velocity (ZSV) and sludge volume index (SVI) of photogranule size classes were determined following Standard Methods (2710D/E).[30] The roundness of photogranules was determined using the software ImageJ.[35]

Statistical analysis. The two-samples *t-test* was performed to determine whether there is a statistically significant difference between variables. Regression analysis was also conducted to examine the relationship between the variables.

RESULTS

Source of photogranules and their size separation. Photogranules were generated in stirred OPG reactors described in Abouhend *et al*.[17] The reactors were seeded with hydrostatically-formed photogranules and operated in sequencing batch mode with a provision of cyclic light, treating primary-effluent wastewater without aeration. Over the first few days of reactor start-up, seed photogranules disintegrated and new biomass aggregates started appearing in the bulk liquid. These proto-photogranules were smaller than 600 μm in diameter.[17] With continuing reactor operation, which included wastewater feeding, discharge of treated water, and regular biomass wastage, the photogranular biomass substantially increased both in number and in size. The size range of the mixed photogranular biomass during the steady-state period was between 0.1 mm and 4.5 mm. For the current study, we used a wet sieving method[28] to sort photogranules into different size groups. Figure 1 shows the images of photogranules separated into seven size classes used in this study: 1) <0.2 mm; 2) 0.2−0.5 mm; 3) 0.5−1 mm; 4) 1−1.7 mm; 5) 1.7−2.5 mm; 6) 2.5−3.5 mm; and 7) 3.5−4.5 mm.

Enrichment of filamentous cyanobacteria during photogranulation. We measured chlorophylls (*a, b* and *c*) and phycobilin and determined their weight fractions in photogranular biomass. As photogranule size increased from the smallest group (<0.2 mm) to the class 0.5−1 mm in diameter, the fraction of chlorophyll *a* in biomass increased from 0.69±0.05% to 1.14±0.08% (Figure 2a), indicating enrichment of phototrophs. For the same size classes, however, chlorophyll *b* and chlorophyll *c* decreased from 0.13±0.01% to 0.12±0.01% and 0.11±0.01% to 0.08±0.01%, respectively (Figures 2b and 2c). These results suggest a decrease in the phototrophic groups producing chlorophyll *b* and chlorophyll *c*, such as green algae and diatoms, respectively. Consequently, the ratios of chlorophyll *a/b* and chlorophyll *a/c* significantly increased from 5.2±0.2 to 9.7±0.7 and 6.4±0.5 to 13.6±1.8, respectively (Figures 2d and 2e).

Similar to chlorophyll *a*, phycobilin increased from 2.9±0.19% to 6.1±0.2%, showing 110% increase, as the photogranule size increased from <0.2 mm to 0.5−1 mm (Figure 2f). The phycobilin/chlorophyll *a* ratio also increased from 4.2±0.3 to 5.4±0.4 (Figure 2g). There were significant differences for the ratio of phycobilin/chlorophyll *a* between the size classes <0.2 mm and 0.2−0.5 mm (p-value 0.001) and between 0.2−0.5 mm and 0.5−1 mm (p-value 0.048). These results suggest that phototrophic enrichment

4

in photogranules up to 0.5–1 mm in diameter was mainly due to the growth of phototrophs that contain chlorophyll *a* and phycobilin, but not chlorophyll *b* and chlorophyll *c*, i.e., cyanobacteria.
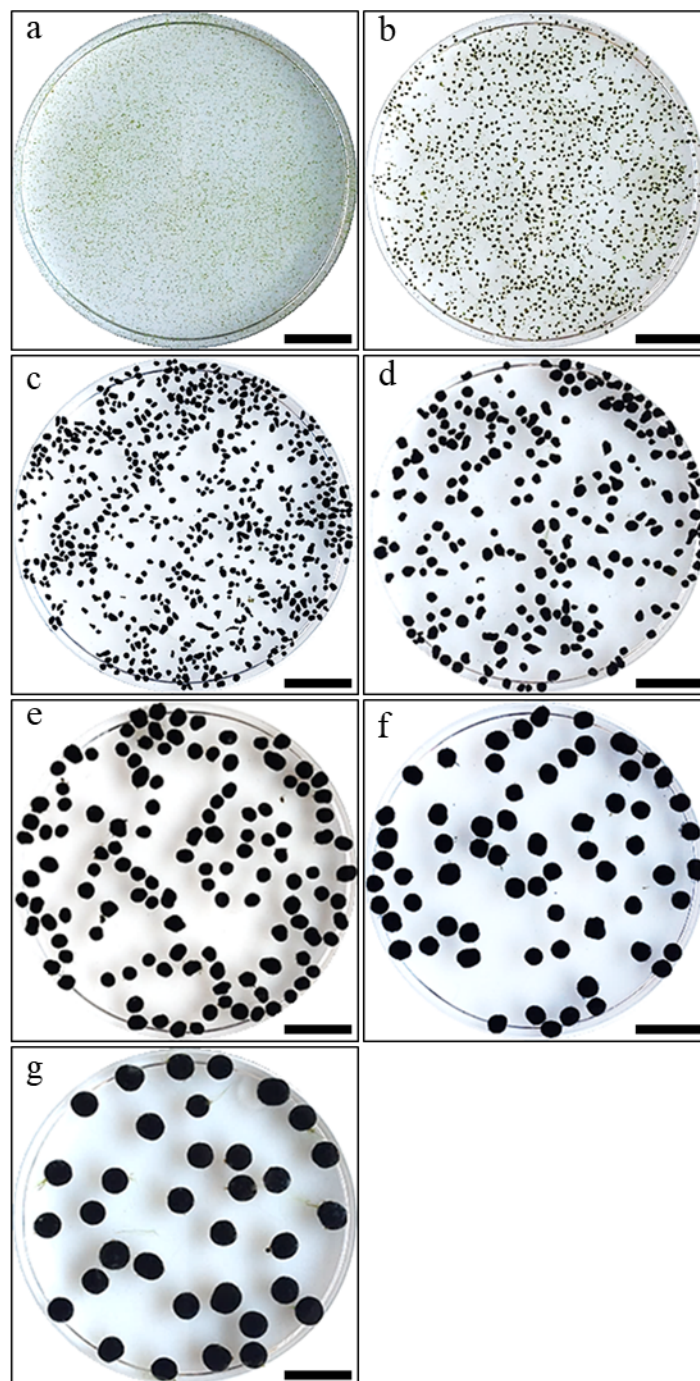

Figure 1. Reactor photogranules classified into seven size groups. (A) Photogranules less than 0.2 mm in diameter. (B–G) Photogranules that fall into the following size ranges. (B) 0.2–0.5 mm in diameter. (C) 0.5–1 mm in diameter. (D) 1–1.7 mm in diameter. (E) 1.7–2.5 mm in diameter. (F) 2.5–3.5 mm in diameter. (G) 3.5–4.5 mm in diameter. Scale bar for all panels is 1 cm.
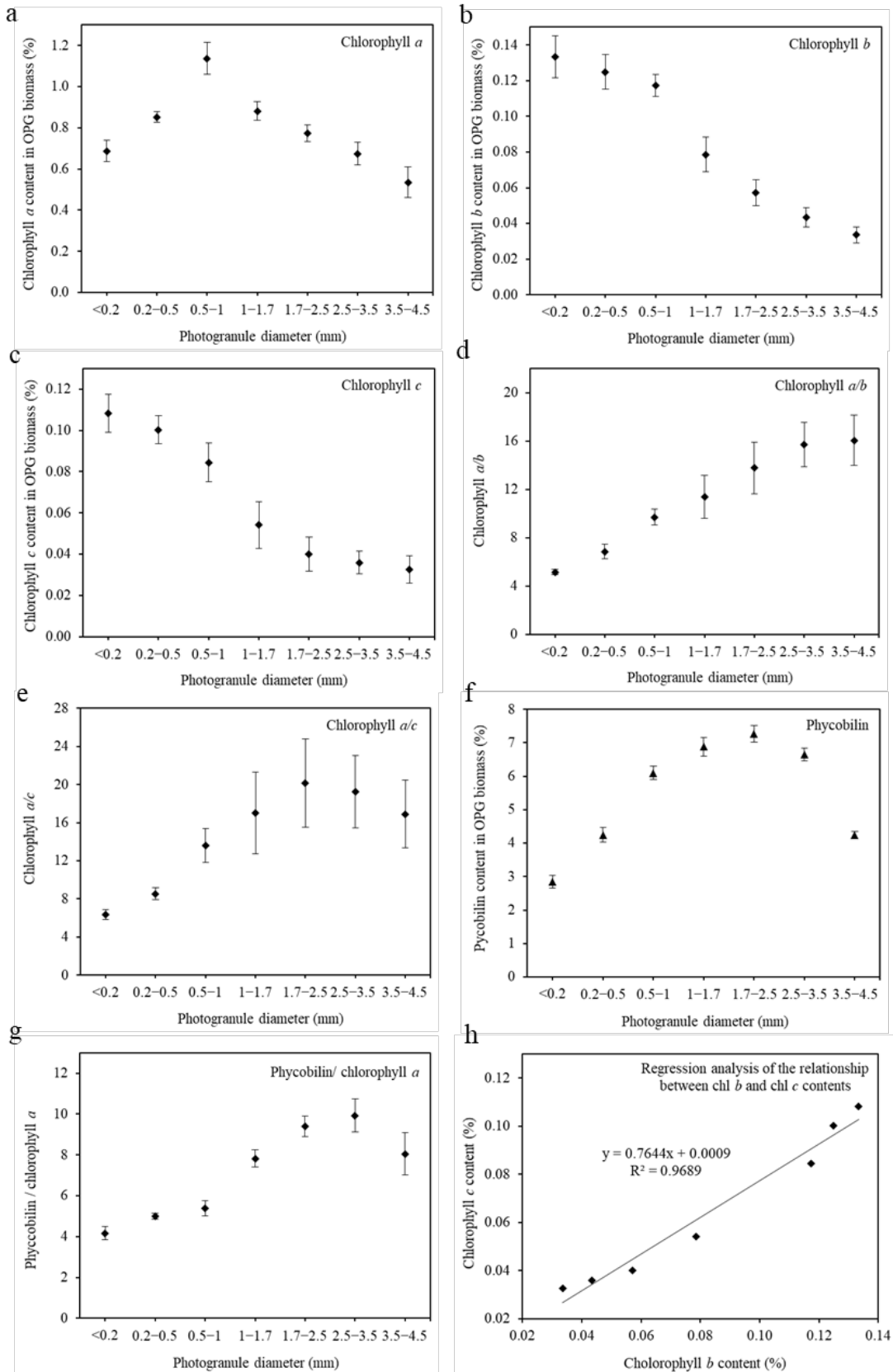
Figure 2. The photosynthetic pigment content in photogranules in different size groups. (A–C) The weight fraction of chlorophyll *a*, chlorophyll *b*, and chlorophyll *c* in photogranular biomass. (D–E) The ratio of chlorophyll *a* to *b* and chlorophyll *a* to *c*. (F) The weight fraction of phycobilin in photogranular biomass. (G) The ratio of phycobilin to chlorophyll *a*. (H) The relationship between the weight fraction of chlorophyll *b* and chlorophyll *c* in photogranular biomass. Error bars represent the standard deviations of triplicate samples.

As the photogranules grow over 0.5–1 mm in diameter, the fraction of chlorophyll *a* in the biomass started to decrease with the size. As the photogranule size increased from 0.5–1 mm to 3.5–4.5 mm, the largest size class in this study, chlorophyll *a* decreased from 1.14±0.08% to 0.54±0.07% (Figure 2a), indicating significant reduction in phototrophic population. The fractions of chlorophyll *b* and chlorophyll *c* continued to decrease over these size classes until they reached 0.03±0.004% and 0.03±0.007%, respectively, in the size class 3.5–4.5 mm in diameter (Figures 2b and 2c). Despite decreases in all chlorophyll contents after class 0.5–1 mm, the chlorophyll *a/b* and chlorophyll *a/c* ratios still show clear increasing trends (Figures 2d and 2e). These results indicate that the decrease in overall phototrophic population (seen by chlorophyll *a*) as the photogranules grow beyond size class 0.5–1 mm is once again due to continuing decreases in the population of phototrophs producing chlorophyll *b* and *c*.

The fraction of phycobilin continued to increase with photogranule size until it reached 7.3±0.3% in the size class 1.7–2.5 mm, indicating enrichment of cyanobacteria in photogranules growing up to this size fraction (Figure 2f). The phycobilin/chlorophyll *a* ratio also increased from 5.4±0.4 to 9.4±0.5 for the same size classes (Figure 2g). As photogranules grow above 1.7–2.5 mm in diameter, the weight fraction of phycobilin started to decrease. Phycobilin decreased from 7.3±0.3% to 4.2±0.1% as the photogranules' diameter increased from 1.7–2.5 mm to 3.5–4.5 mm (Figure 2f). The fraction of phycobilin in photogranules was significantly different between size classes 1.7–2.5 mm and 2.5–3.5 mm (p-value 0.03) and between 2.5–3.5 mm and 3.5–4.5 mm (p-value 0.0002). These results suggest that the relative population of cyanobacteria in photogranules also becomes smaller once the photogranules grow above 1.7–2.5 mm, especially above 2.5–3.5 mm in diameter.

Among seven size classes, the size class 0.5–1 mm showed the highest content of chlorophyll *a* (1.14±0.08%) while the size class <0.2 mm showed the highest fraction of chlorophyll *b* and *c* (0.13±0.01% and 0.11±0.01%, respectively). The size class 3.5–4.5 mm showed the lowest content of all chlorophylls. Chlorophyll *b* and chlorophyll *c* showed a strong positive correlation (R^2 = 0.97, Figure 2h). For phycobilin, the size class <0.2 mm showed the lowest fraction (2.9±0.19%) and the size class 1.7–2.5 mm showed the highest fraction (7.3±0.26%). These results suggest that the phototrophic community in photogranules shift from green algae/diatoms in the smaller photogranules to cyanobacteria in the larger photogranules.

Structural development of photogranules. The biomass in the smallest size class (<0.2 mm in diameter) showed an average roundness of 0.55±0.11, indicating non-spherical aggregates (Figure S1). As the size of photogranules increased from <0.2 mm to 3.5–4.5 mm, the roundness increased from 0.55±0.11 to 0.93±0.06, indicating that the photogranular biomass becomes more spherical as it grows larger. Microscopic analysis showed that the surface roughness of photogranules also changes as they grow bigger (Figure 3). The surface of photogranules changed from hairy nature to smooth one as the photogranule size increases from <0.2 mm to 3.5–4.5 mm. The color of photogranules also changed from light green to dark blue green as their size increased (Figure 1). It can be inferred that the change in the photogranules' color occurred along with the changes in pigment content and enrichment of cyanobacteria within the photogranules (Figure 2).
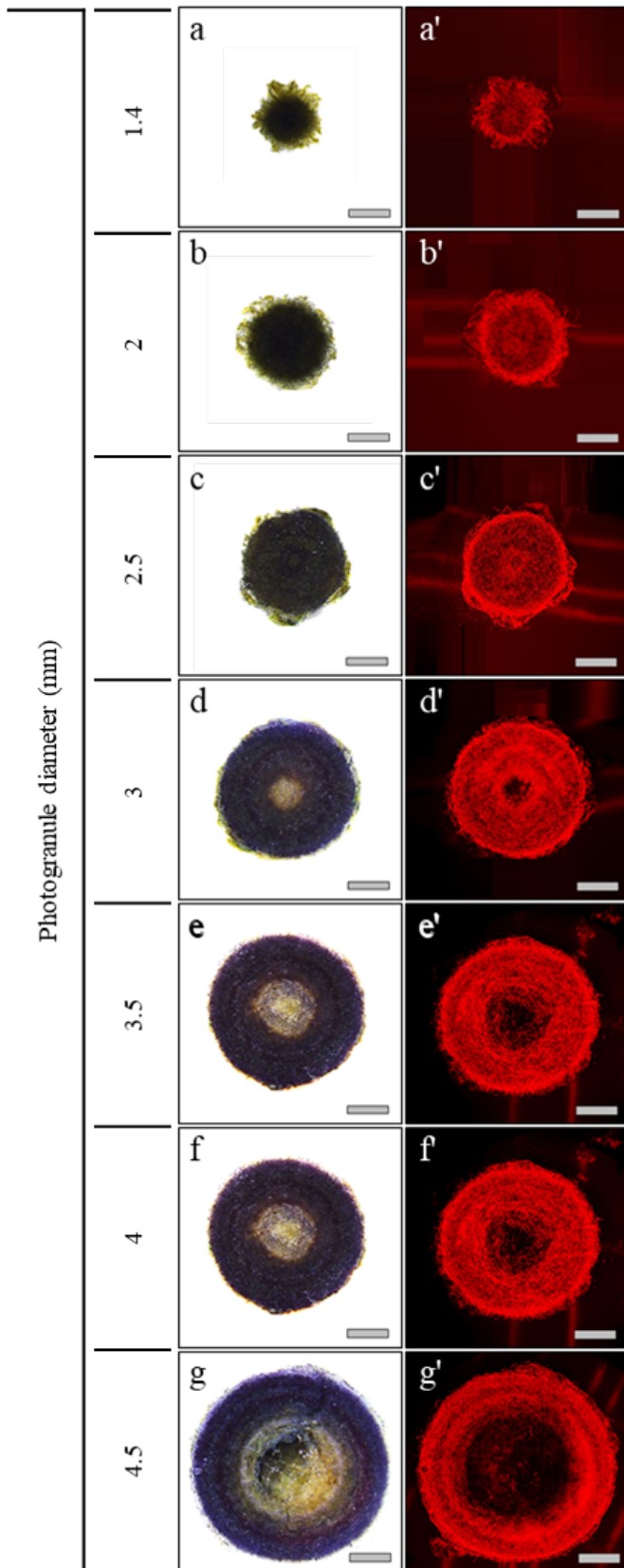
Figure 3. Microscopic images showing the structural development of photogranules produced in sequencing batch reactors treating primary-effluent wastewater without aeration. (A−G) Cross-sections of photogranules viewed by brightfield light microscopy. (A'−G') The same cross-sections of photogranules viewed by phycocyanin autofluorescence of cyanobacteria. The images reveal the development of a cyanobacterial layer of 1.25±0.14 mm thickness in photogranules ≥3 mm in diameter. Scale bar for all panels is 1 mm.

As seen with the brightfield and phycocyanin autofluorescence microscopy of cross-sectioned photogranules (Figure 3), the photogranules underwent sequential structural changes as they evolved into larger sizes. In photogranules smaller than 3 mm in diameter, filamentous cyanobacteria were spread over the whole body (Figures 3a–c and 3a'–c'). Scanning electron microscopy (SEM) also showed that high level of filamentous cyanobacteria are located across the granular body in photogranules <3 mm in diameter (Figure 4a–c; Figure S2a–c). Photogranules of 3 mm in diameter and above showed a distinct layered structure where a mat-like outer layer of filamentous cyanobacteria encloses non-cyanobacterial core biomass (Figures 3d–g and 3d'–g'). SEM also revealed that filamentous cyanobacteria dominate the outer layer of these large photogranules while the filamentous cyanobacteria are basically absent in the core center of photogranules (Figure 4d–f; Figure S2d–f). In this core, diatoms and unicellular green algae were more readily observed along with EPS-like matter (Figure 4f; Figure S2d–f). In addition, many fragments of dead diatoms were observed in the center of these large-size photogranules (Figure S2e).
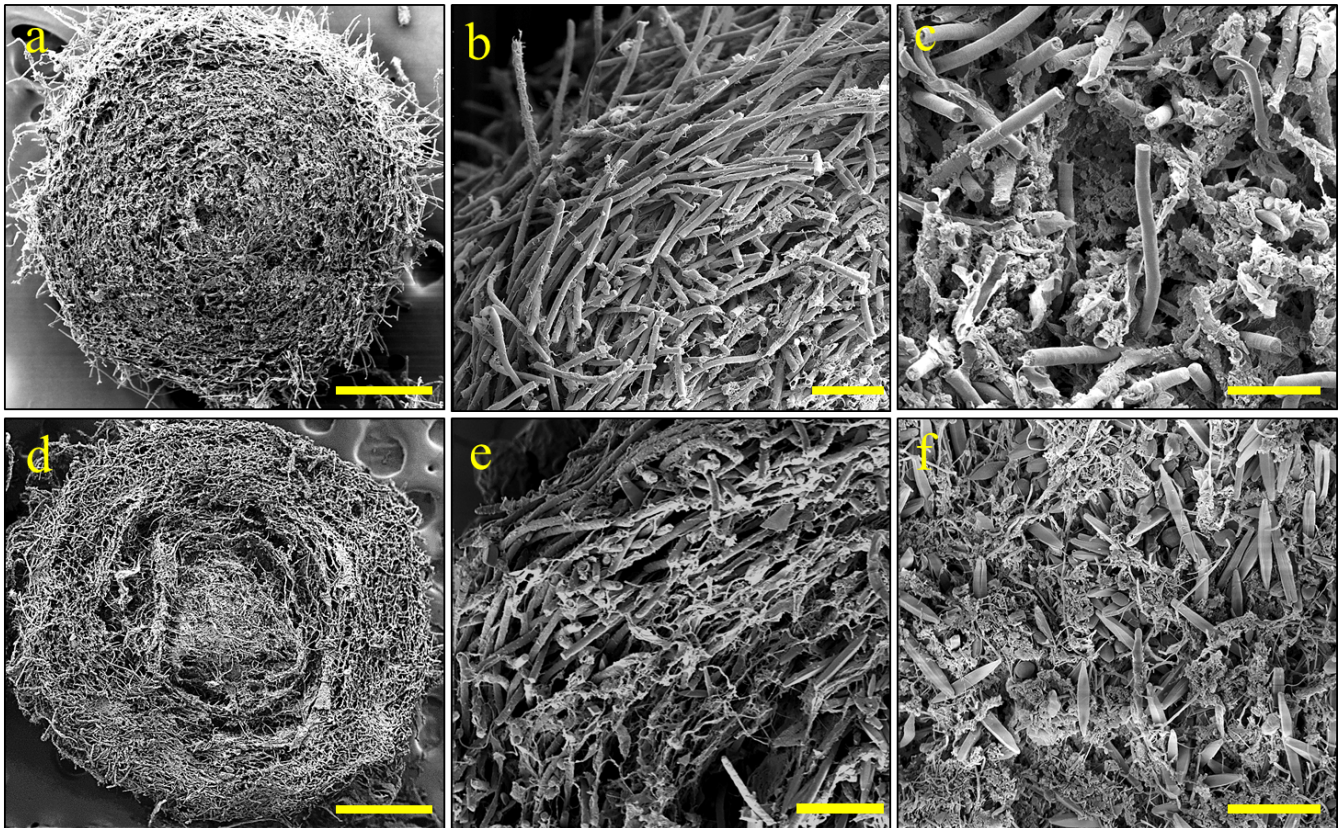

Figure 4. Scanning electron microscopy (SEM) of cross-sectioned photogranules of two different sizes. (A) Cross-section of a small photogranule, approximately 1 mm in diameter. (B) Cyanobacterial outer layer of the same photogranule shown in panel (A). (C) The center of the same photogranule shown in panel (A). (D) Cross-section of a large photogranule, approximately 4 mm in diameter. (E) Cyanobacterial outer layer of the same photogranule shown in panel (D). (F) The center of the same photogranule shown in panel (D). Scale bars for panels are (A): 250 μm; (B) and (E): 50 μm; (C) and (F): 25 μm; and (D): 1 mm.

The diameter of the non-cyanobacterial core increased linearly as the size of photogranules increased from 3 mm to 4.5 mm (Figure S3a). The volume fraction of non-cyanobacterial core consequently increased from 0.6±0.3% to 10.7±1.9%, suggesting repression of filamentous cyanobacteria in the photogranules greater than 3 mm (Figure S3b). These results are consistent with the phycobilin data that showed that the weight fraction of phycobilin starts decreasing from the size class 2.5–3.5 mm in diameter. This is also supported by the unchanged depth of the cyanobacterial layer despite the increase in the size of photogranules above 3 mm in diameter (Figure S3c). In photogranules of 3–4.5 mm in diameter, the thickness of the cyanobacterial layer remained constant at 1.25±0.14 mm. In a spherical structure, this would mean a total depth of 2.5 mm for cyanobacterial growth, which is consistent with Figure 3c' showing that in this size of photogranules, filamentous cyanobacteria can be located anywhere in the photogranules.
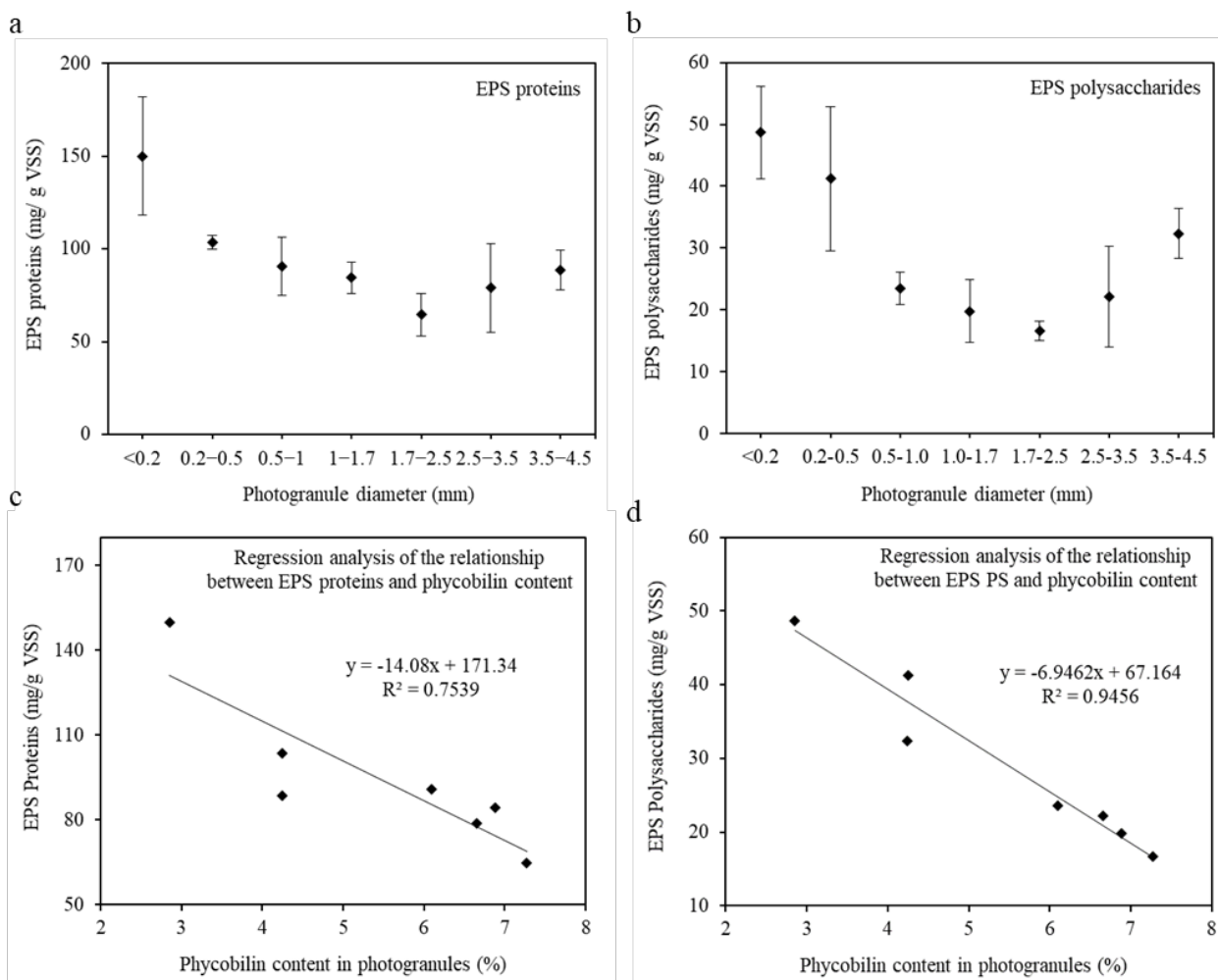
Figure 5. Biomass-bound extracellular polymeric substances (EPS) in photogranules of different size classes. (A) EPS proteins. (B) EPS polysaccharides. (C) The relationship between the quantity of EPS proteins and the weight fraction of phycobilin in photogranules. (D) The relationship between the quantity of EPS polysaccharides and the weight fraction of phycobilin in photogranules. Error bars represent the standard deviations of triplicate measurements.

EPS in photogranules. Concentrations of both EPS proteins and polysaccharides showed a clear decreasing trend as the photogranules grow in size (Figure 5). EPS proteins decreased from 150±32 mg/g volatile suspended solids (VSS) to 65±11 mg/g VSS as the photogranules grow from the size class <0.2 mm to the size class 1.7−2.5 mm (Figure 5a). For the same size classes, EPS polysaccharides decreased from 49±7 mg/g VSS to 17±2 mg/g VSS (Figure 5b). However, both EPS proteins and polysaccharides also increased back once the photogranules grow above 1.7−2.5 mm. As the photogranule size increased from 1.7−2.5 mm to 3.5−4.5 mm, EPS proteins and polysaccharides increased to 89±11 mg/g VSS and 32±4 mg/g VSS, respectively (Figures 5a and 6b). The levels of EPS proteins between size classes 1.7−2.5 mm and 3.5−4.5 mm are likely different (p-value 0.057). Also, statistically significant differences exist between the levels of EPS polysaccharides in size classes 1.7−2.5 mm and 3.5−4.5 mm (p-value 0.01). We found moderate to strong negative relationships between EPS and phycobilin: EPS proteins and phycobilin (R^2 = 0.75, Figure 5c); EPS polysaccharides and phycobilin (R^2 = 0.95, Figure 5d). Thus, the greater the density of cyanobacteria, the less the amount of EPS, especially polysaccharides, in photogranules. It is important to note that the increase in EPS proteins and polysaccharides from the size class 2.5−3.5 mm coincided with the decrease in the weight fraction of phycobilin (Figure 2f) and the development of a layered structure within the photogranules (Figure 3).

Oxygen production by photogranules at different sizes. To study how the photogranules' size affects their oxygen-producing capability, we determined the oxygen production rate (OPR) of photogranular biomass from different size groups. Figure 6a shows the specific oxygen production rate (SOPR) of photogranules in different size classes. SOPR initially increased from 10.9±0.8 to 21.9±1.3 mg O_2/g VSS-h as the photogranule size increased from <0.2 mm to 0.5−1 mm. SOPR then decreased to 8.1±0.5 mg O_2/g VSS-h along with the increase in photogranule size from 0.5−1 mm to 3.5−4.5 mm. The SOPR correlated very strongly with the weight fraction of chlorophyll *a* in photogranules (R^2 = 0.99, Figure 6b). Among seven size classes, photogranules in the size range of 0.5−1 mm showed the highest SOPR, on average, 21.9±1.3 mg O_2/g VSS-h. This SOPR was much greater than the SOPR of mixed photogranular biomass collected from the same reactor, which showed, on average, 12.6±2.4 mg O_2/g VSS-h.

Settleability of photogranules. Effective separation of biomass from water is also an advantage of the OPG process for wastewater treatment. We determined ZSV and SVI to study how the photogranules' growth in size impacts their settling properties. ZSV of photogranules gradually, and substantially, increased from 3±1.6 m/h to 78.4±4.1 m/h, as the photogranules grow from <0.2 mm to 3.5−4.5 mm (Figure S4a). SVI decreased from 383±5 mL/g VSS to 39±2.8 mL/g VSS, as the size class of photogranules increased from <0.2 mm to 1−1.7 mm, strong indication of progression of granulation (Figure S4b). The ZSV and SVI of the size class 0.5−1 mm, which showed the highest oxygen production rate, were 24.6±5 m/h and 40.5±2.8 mL/g VSS, respectively. These values are more favorable for operation compared to ZSV and SVI observed for the mixed photogranular biomass, 14.6±0.5 m/h and 53±2 mL/g VSS, respectively.
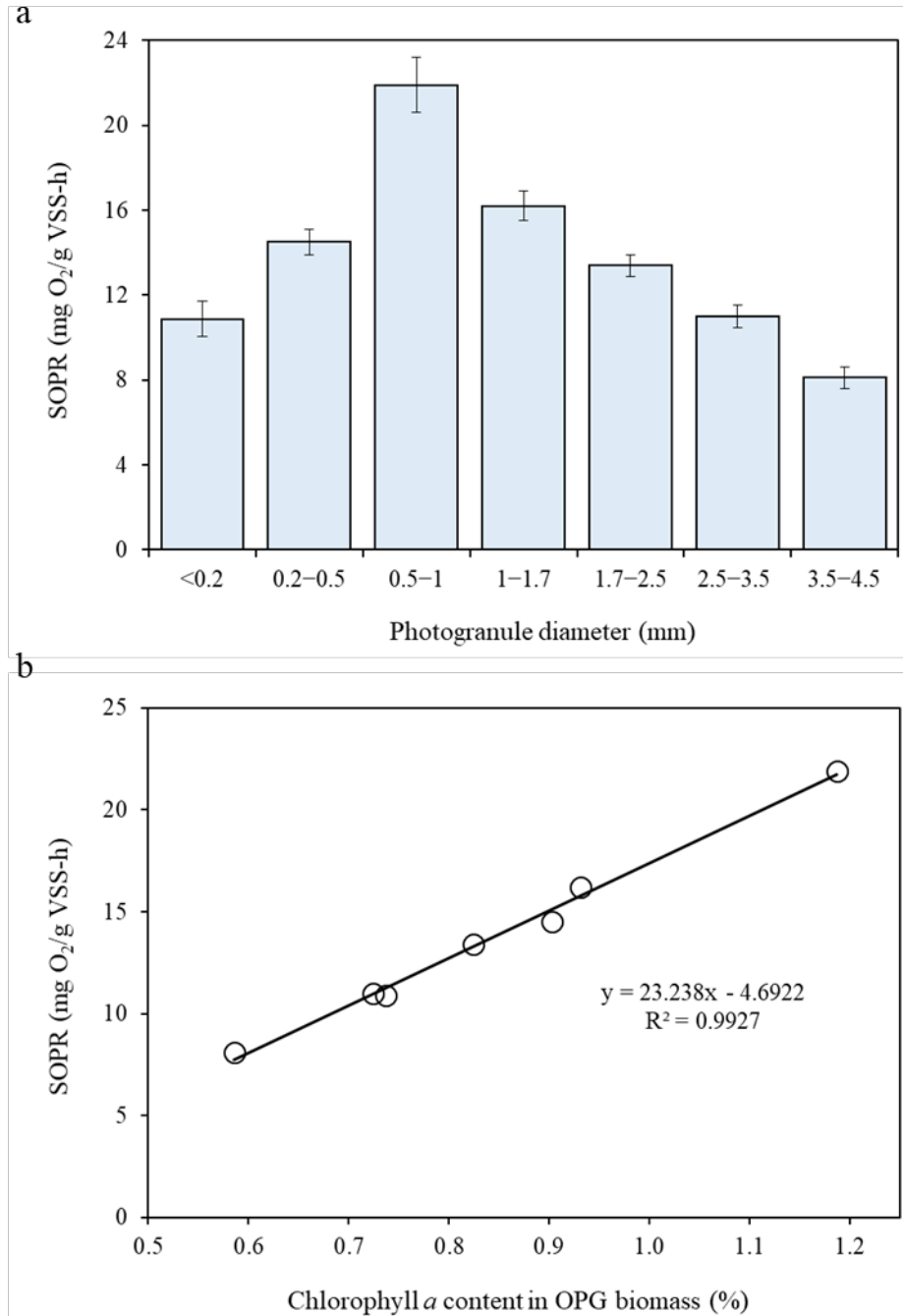
Figure 6. The specific oxygen production rate (SOPR) of different photogranule size classes and its correlation to chlorophyll *a* content in photogranules. (A) SOPR. (B) Regression analysis showing a linear relationship between SOPR and the weight fraction of chlorophyll *a* in photogranules. SOPR represents the net oxygen production rate plus the theoretical oxygen demand for the oxidation of organic matter and nitrification in closed batch normalized by biomass concentration. Error bars represent the standard deviations of triplicate samples.

DISCUSSION

Photogranules, like any other granules, grow in reactor systems via two means: the number and the size. While we previously showed the growth of photogranules from the reactor's mixed biomass standpoint,[17] how an individual photogranule grows to a larger size and how this change would impact the system performance has remained mainly unknown. The current study focuses on these important matters, by investigating the physicochemical and biological characteristics of photogranules in different sizes and their capability of producing O_2, the key property of the OPG process for wastewater treatment.

We found that the photogranules' growth in size occurs along with the change in phototrophic community. The mass fraction of chlorophyll *b* and chlorophyll *c* showed clear decreasing trends with increase in photogranule size (Figures 2b and 2c), suggesting a decrease in abundance of green algae and diatoms, respectively, and development of unfavorable conditions for these community as photogranules grow. A strong positive correlation found between chlorophyll *b* and chlorophyll *c* (Figure 2h) also indicates that these phototrophic community experienced a similar fate along with size progression in photogranules.

In contrast to green algae and diatoms, the growth of filamentous cyanobacteria was promoted during the size evolution of photogranules occurring in reactors. Both chlorophyll (*a*, *b*, *c*, *a/b*, and *a/c*) and phycobilin data showed that the growth of photogranules up to 1.7–2.5 mm in diameter continued with the enrichment of cyanobacteria. Once the photogranules exceed this size, the photogranules' cyanobacterial fraction also started to decrease. It is important to note that this decrease coincides with the appearance of a layered structure in the photogranules in which a concentric cyanobacterial layer encloses non-cyanobacterial core biomass (Figure 3).

We currently postulate that the development of this layered structure is caused by migration of filamentous cyanobacteria towards the photogranules' surface, because as the photogranules grow larger, light inside the photogranules should become more limited. Literature shows that subsection III filamentous cyanobacteria, the main cyanobacterial group enriched in photogranules,[10] exhibit phototaxis, which is a movement in response to light.[36–38] It is well known that these filamentous cyanobacteria secret and use EPS for their gliding motility.[39–41] These are consistent with our observation that EPS polysaccharides and proteins, especially the former, significantly increase along with the development of the layered structure (Figures 5a and 5b). These observations are also consistent with what Kuo-Dahab *et al*.[19] found with the formation of photogranules from activated sludge under hydrostatic conditions. Kuo-Dahab *et al*.[19] showed increase in EPS polysaccharides during this photogranulation process, and further showed that copious amounts of slimes and sheaths are closely associated with filamentous cyanobacteria in the outer layer of hydrostatically-formed photogranules.

The gliding mobility would, therefore, provide clear advantage to filamentous cyanobacteria over green algae and diatoms during the size evolution of photogranules, which would result in limited light inside the photogranules. Nevertheless, the depth of the cyanobacterial layer remains unchanged although the photogranules continued to grow above 3 mm in diameter (Figure S3c). This observation suggests that there is a maximum depth limiting the growth of filamentous cyanobacteria in photogranules. This means as the photogranules continue to grow bigger, the fraction of filamentous cyanobacteria in photogranules becomes smaller, which will ultimately lead to the point where the structure of photogranules may not be sustained. The maximum size of photogranules in this study, however, could have been greater if we had used a lower hydraulic shear force to mix the system. There are several lines of discussion to support this statement. First, the volume fraction of the cyanobacterial layer in photogranules at 4.5 mm in diameter is approximately 90%, which is still substantially greater

than the volume fraction of non-cyanobacterial aggregates. Furthermore, hydrostatically-formed photogranules reported are much larger than the size of photogranules grown in the reactors. Finally, our ongoing reactor study showed that the photogranules growing in reactors with mixing at 50 rpm (while other operational conditions remain same as the current study) grow up to approximately 5.5 mm in diameter.

The layered structure in photogranules looks similar to that in microbial mats.[41–44] Nevertheless, photogranules self-organize and grow into a spherical aggregate, whereas mats are formed on a planar solid surface. As discussed by Milferstedt et al.[10] granules similar to photogranules also appear in glacier environments. Cryoconites that form in the melt holes of glacier surfaces are also spherical or sphere-like granules in which filamentous cyanobacteria serve as a key granulating species.[6–8,45] The layered structure observed in photogranules also appears in cryoconite granules.[6] The outer layer thickness in cryoconite granules varied among different granules, but is generally about 0.2 mm on average.[6] This suggests that photogranules and cryoconite granules share the formation mechanism despite extremely different environments in which the growth of these granules occurs. Notably, photogranules are organic rich whereas cryoconite granules are mineral rich[6–8] and can contain inorganic matter even up to 98%.[8] This again suggests that conditions under which these two granule types are generated are substantially different. Knowing the environmental (macro and micro) conditions and biological responses necessary to not only select filamentous cyanobacteria but also induce their physiology leading to a common granular morphology will thus be important to understand the formation of both photogranules and cryoconite granules. We believe this warrants future investigation.

The OPG process is a self-aerating wastewater treatment system where the photogranular biomass produces the oxygen required for the oxidation of organic matter and nitrification.[10,17] Therefore, the oxygen production capacity of the photogranular biomass is a key design consideration in the OPG process. In this study, the OPR of photogranules was determined based on the direct measurements of dissolved O_2 in closed bottles as well as the theoretical amount of oxygen required for the oxidation of organic matter and nitrification. The generation of dissolved O_2 in closed systems indicates the diffusion of O_2 from the body of photogranules into bulk liquid. Hann et al.[46] also showed the gradient of dissolved O_2 established within the photogranules where the level of dissolved O_2 decreases with depth, suggesting diffusion of oxygen from the outer layer toward the center of photogranules. These outward and inward oxygen diffusions are absent in other microbial granules. For example, in aerobic granule sludge, oxygen is always provided from the external source and diffuses from the bulk liquid into the granule.[24,26,27]

Our results showed that photogranule size has large influence on the biomass's capability of producing oxygen and, thus, its treatment potential. Photogranules in the size class 0.5−1 mm showed the highest oxygen production rate, which is 1.4 to 2.7 times greater than that from other size classes. Earlier, Abouhend et al.[17] reported the performance of the OPG systems treating real wastewater along with the evolution of photogranule size over five-months period. During day 50 to day 60, when the majority of photogranular biomass was in the range of 0.5−1 mm with a mean size of 0.75 mm, the reactors showed the efficiency of total COD (tCOD) removal at 88±3%. During the same operation period, effluents tCOD was, on average, 16±5 mg/L, suggesting high effluent quality. This tCOD removal was significantly higher than the removal observed during earlier or later operation periods when the mean size of biomass, based on both number and biovolume of photogranules in reactors, was smaller than 0.5 mm or larger than 1 mm: 78±7% and 79±5%, respectively. These observations, therefore, suggest

that the treatment capacity of the OPG systems will be influenced by photogranule size and the oxygenic function of photogranules.

A very strong correlation between SOPR and the fraction of chlorophyll *a* in the photogranular biomass (Figure 6b) indicates that the photogranules' oxygen production is directly determined by the relative population of phototrophic organisms. The size progression to the size class 0.5−1 mm, showing the highest SOPR among seven size classes, occurs with significant increase in the fraction of phycobilin but decrease in the fraction of chlorophyll *b* and chlorophyll *c*. Further development to the size class 1−1.7 mm, the group with the second highest SOPR, came along with continuous increase in phycobilin yet substantial decrease in chlorophyll *b* and chlorophyll *c*, indicative of maturation in photogranulation with the enrichment of filamentous cyanobacteria. Hence, photogranules in these two size groups, i.e., photogranules in 0.5−1.7 mm in diameter, would be optimal for the OPG process with respect to both oxygen production (thus, treatment capacity) and the stability or maturity of photogranules. It can also be inferred that the photogranule size greater than 2.5 mm in diameter in which relative cyanobacterial population further decreases and the layered structure starts to develop will not be as effective as smaller photogranules in terms of aerobic treatment. These bigger photogranules may be exploited for nitrogen removal based on simultaneous nitrification and denitrification (SND) based on the formation of stratified structure and the presence of both oxic and anoxic environments within the same biomass. According to Abouhend *et al.*,[17] however, nitrogen removal by SND pathway seems negligible since major nitrogen removal in the OPG systems occurred via bioassimilation and denitrification occurring during the dark cycle (i.e., no light and no oxygen). Nonetheless, the occurrence of SND-based nitrogen removal by different size photogranules may need more investigation.

The results of the current study are expected to help us to engineer the OPG process by maintaining the optimal photogranule size in the system and, thus, operating the OPG system at high treatment efficiency and stability with respect to granulation. Maintaining the optimal size range of photogranules in the OPG system can be achieved by multiple ways. One could be introducing intermittent high shear in the reactor. For aerobic granular sludge, increasing hydrodynamic shear in reactors has been proposed to suppress the overgrowth of large granules.[21] Other approaches could be using devices that enable separation of biomass based on size, such as screening and hydrocyclone, which can be installed in the recycling line of an OPG system. As the growth rate of photogranules is expected to be different depending on photogranule size, operating the system with selective biomass removal should consider the photogranule's growth rate and its effect on the effectiveness of photogranulation. The future research will need to examine the hypothesis that controlling the photogranular biomass size will optimize the photogranules' oxygenic function and system performance in reactor operation. Collectively, engineering the OPG system based on better understanding of photogranules' growth and function is expected to advance the development of a new granular technology, which has potential to treat wastewater without energy intensive aeration.

REFERENCES

1   Boedeker, C.; Immers, A. No More Lake Balls (Aegagropila Linnaei Kützing, Cladophorophyceae, Chlorophyta) in The Netherlands? *Aquat. Ecol.* **2009**, *43* (4), 891–902.

2   Brehm, U. P. Laboratory cultures of calcifying biomicrospheres generate ooids - A contribution to the origin of oolites. *Carnets de Géologie/Notebooks on Geology Maintenon Letter* **2004**, (3), 1–6.

3   Brehm, U.; Krumbein, W. E.; Palinska, K. A. Biomicrospheres Generate Ooids in the Laboratory. *Geomicrobio. J.* **2006**, *23* (7), 545–550.

4   Malin, G.; Pearson, H. W. Aerobic Nitrogen Fixation in Aggregate-Forming Cultures of the Nonheterocystous Cyanobacterium Microcoleus Chthonoplastes. *Microbiology* **1988**, *134* (7), 1755–1763.

5   Capone, D. G.; Zehr, J. P.; Paerl, H. W.; Bergman, B.; Carpenter, E. J. Trichodesmium, a Globally Significant Marine Cyanobacterium. *Science* **1997**, *276* (5316), 1221–1229.

6   Takeuchi, N.; Kohshima, S.; Seko, K. Structure, Formation, and Darkening Process of Albedo-Reducing Material (Cryoconite) on a Himalayan Glacier: A Granular Algal Mat Growing on the Glacier. *Arct. Antarct. Alp. Res.* **2001**, *33* (2), 115–122.

7   Langford, H.; Hodson, A.; Banwart, S.; Bøggild, C. The Microstructure and Biogeochemistry of Arctic Cryoconite Granules. *Ann. Glaciol.* **2010**, *51* (56), 87–94.

8   Cook, J.; Edwards, A.; Takeuchi, N.; Irvine-Fynn, T. Cryoconite: The Dark Biological Secret of the Cryosphere. *Prog. Phys. Geogr.* **2016**, *40* (1), 66–111.

9   Park, C.; Dolan, S. Algal-Sludge Granule for Wastewater Treatment and Bioenergy Feedstock Generation. Patent cooperation treaty, 2105, WO/2015/112654, July 31.

10   Milferstedt, K.; Kuo-Dahab, W. C.; Butler, C. S.; Hamelin, J.; Abouhend, A. S.; Stauch-White, K.; McNair, A.; Watt, C.; Carbajal-González, B. I.; Dolan, S.; et al. The Importance of Filamentous Cyanobacteria in the Development of Oxygenic Photogranules. *Sci. Rep.* **2017**, *7* (1), 17944.

11   Tiron, O.; Bumbac, C.; Manea, E.; Stefanescu, M.; Nita Lazar, M. Overcoming Microalgae Harvesting Barrier by Activated Algae Granules. *Sci. Rep.* **2017**, *7* (1), 4646.

12   Huang, W.; Li, B.; Zhang, C.; Zhang, Z.; Lei, Z.; Lu, B.; Zhou, B. Effect of Algae Growth on Aerobic Granulation and Nutrients Removal from Synthetic Wastewater by Using Sequencing Batch Reactors. *Bioresour. Technol.* **2015**, *179*, 187–192.

13   Quijano, G.; Arcila, J. S.; Buitrón, G. Microalgal-Bacterial Aggregates: Applications and Perspectives for Wastewater Treatment. *Biotechnol. Adv.* **2017**, *35* (6), 772–781.

14   Van Den Hende, S.; Laurent, C.; Bégué, M. Anaerobic Digestion of Microalgal Bacterial Flocs from a Raceway Pond Treating Aquaculture Wastewater: Need for a Biorefinery. *Bioresour. Technol.* **2015**, *196*, 184–193.

15   Ahmad, J. S. M.; Cai, W.; Zhao, Z.; Zhang, Z.; Shimizu, K.; Lei, Z.; Lee, D.-J. Stability of Algal-Bacterial Granules in Continuous-Flow Reactors to Treat Varying Strength Domestic Wastewater. *Bioresour. Technol.* **2017**, *244*, 225–233.

16   Zhang, B.; Lens, P. N. L.; Shi, W.; Zhang, R.; Zhang, Z.; Guo, Y.; Bao, X.; Cui, F. Enhancement of Aerobic Granulation and Nutrient Removal by an Algal–Bacterial Consortium in a Lab-Scale Photobioreactor. *Chem. Eng. J.* **2018**, *334*, 2373–2382.

17   Abouhend, A. S.; McNair, A.; Kuo-Dahab, W. C.; Watt, C.; Butler, C. S.; Milferstedt, K.; Hamelin, J.; Seo, J.; Gikonyo, G. J.; El-Moselhy, K. M.; Park, C. The Oxygenic Photogranule Process for Aeration-Free Wastewater Treatment. *Environ. Sci. Technol.* **2018**, *52* (6), 3503–3511.

18 Ansari, A. A.; Abouhend, A. S.; Park, C. Effects of Seeding Density on Photogranulation and the Start-up of the Oxygenic Photogranule Process for Aeration-Free Wastewater Treatment. *Algal Res.* **2019**, *40*, 101495.

19 Kuo-Dahab, W. C.; Stauch-White, K.; Butler, C. S.; Gikonyo, G. J.; Carbajal-González, B.; Ivanova, A.; Dolan, S.; Park, C. Investigation of the Fate and Dynamics of Extracellular Polymeric Substances (EPS) during Sludge-Based Photogranulation under Hydrostatic Conditions. *Environ. Sci. Technol.* **2018**, *52* (18), 10462–10471.

20 Stauch-White, K.; Srinivasan, V. N.; Camilla Kuo-Dahab, W.; Park, C.; Butler, C. S. The Role of Inorganic Nitrogen in Successful Formation of Granular Biofilms for Wastewater Treatment That Support Cyanobacteria and Bacteria. *AMB Expr.* **2017**, *7* (1), 146.

21 Zhou, J.; Zhang, Z.; Zhao, H.; Yu, H.; Alvarez, P. J. J.; Xu, X.; Zhu, L. Optimizing Granules Size Distribution for Aerobic Granular Sludge Stability: Effect of a Novel Funnel-Shaped Internals on Hydraulic Shear Stress. *Bioresour. Technol.* **2016**, *216*, 562–570.

22 Dahalan, F. A.; Abdullah, N.; Yuzir, A.; Olsson, G.; Salmiati; Hamdzah, M.; Din, M. F. M.; Ahmad, S. A.; Khalil, K. A.; Anuar, A. N.; et al. A Proposed Aerobic Granules Size Development Scheme for Aerobic Granulation Process. *Bioresour. Technol.* **2015**, *181*, 291–296.

23 Toh, S.; Tay, J.; Moy, B.; Ivanov, V.; Tay, S. Size-Effect on the Physical Characteristics of the Aerobic Granule in a SBR. *Appl. Microbiol. Biotechnol.* **2003**, *60* (6), 687–695.

24 Li, Y.; Liu, Y. Diffusion of Substrate and Oxygen in Aerobic Granule. *Biochem. Eng. J.* **2005**, *27* (1), 45–52.

25 Fang, F.; Qiao, L.-L.; Ni, B.-J.; Cao, J.-S.; Yu, H.-Q. Quantitative Evaluation on the Characteristics of Activated Sludge Granules and Flocs Using a Fuzzy Entropy-Based Approach. *Sci. Rep.* **2017**, *7*, 42910.

26 Chiu, Z. C.; Chen, M. Y.; Lee, D. J.; Wang, C. H.; Lai, J. Y. Oxygen Diffusion and Consumption in Active Aerobic Granules of Heterogeneous Structure. *Appl. Microbiol. Biotechnol.* **2007**, *75* (3), 685–691.

27 Su, K.-Z.; Yu, H.-Q. A Generalized Model for Aerobic Granule-Based Sequencing Batch Reactor. 1. Model Development. *Environ. Sci. Technol.* **2006**, *40* (15), 4703–4708.

28 Selbig, W. Use of wet sieving to improve the accuracy of sediment and sediment-associated constituent concentrations in whole-water samples. *Proceeding of the 8th Federal Interagency Sedimentation Conference* **2006**.

29 Baskin, T. I.; Orr, T. J.; Jercinovic, M.; Yoshida, M. Sample Preparation for Scanning Electron Microscopy: The Surprising Case of Freeze Drying from Tertiary Butanol. *Microscopy Today* **2014**, *22* (3), 36–39.

30 Association, A. P. H. *Standard Methods for the Examination of Water & Wastewater*; American Public Health Association, 2005.

31 Bennett, A.; Bogorad, L. Complementary Chromatic Adaptation in a Filamentous Blue-Green Alga. *J. Cell Biol.* **1973**, *58* (2), 419–435.

32 Islam, M. A.; Beardall, J. Growth and Photosynthetic Characteristics of Toxic and Non-Toxic Strains of the Cyanobacteria Microcystis Aeruginosa and Anabaena Circinalis in Relation to Light. *Microorganisms* **2017**, *5* (3).

33 DuBois, Michel.; Gilles, K. A.; Hamilton, J. K.; Rebers, P. A.; Smith, Fred. Colorimetric Method for Determination of Sugars and Related Substances. *Anal. Chem.* **1956**, *28* (3), 350–356.

34 Frølund, B.; Palmgren, R.; Keiding, K.; Nielsen, P. H. Extraction of Extracellular Polymers from Activated Sludge Using a Cation Exchange Resin. *Water Res.* **1996**, *30* (8), 1749–1758.

35 Schneider, C. A.; Rasband, W. S.; Eliceiri, K. W. NIH Image to ImageJ: 25 Years of Image Analysis. *Nat. Methods* **2012**, *9* (7), 671–675.

36 Castenholz, R. W. Aggregation in a Thermophilic Oscillatoria. *Nature* **1967**, *215* (5107), 1285.

37 Castenholz, R. W.; Jørgensen, B. B.; D'Amelio, E.; Bauld, J. Photosynthetic and Behavioral Versatility of the Cyanobacterium Oscillatoria Boryana in a Sulfide-Rich Microbial Mat. *FEMS Microbiol. Ecol.* **1991**, *9* (1), 43–57.

38 Biddanda, B. A.; McMillan, A. C.; Long, S. A.; Snider, M. J.; Weinke, A. D. Seeking Sunlight: Rapid Phototactic Motility of Filamentous Mat-Forming Cyanobacteria Optimize Photosynthesis and Enhance Carbon Burial in Lake Huron's Submerged Sinkholes. *Front. Microbiol*. **2015**, *6*, 930.

39 Hoiczyk, E.; Baumeister, W. Envelope Structure of Four Gliding Filamentous Cyanobacteria. *J Bacteriol.* **1995**, *177* (9), 2387–2395.

40 Hoiczyk, E. Gliding Motility in Cyanobacterial: Observations and Possible Explanations. *Arch. Microbiol.* **2000**, *174* (1–2), 11–17.

41 *The Ecology of Cyanobacteria: Their Diversity in Time and Space*; Whitton, B. A., Potts, M., Eds.; Springer Netherlands, 2002.

42 Pierson, B. K.; Parenteau, M. N. Phototrophs in High Iron Microbial Mats: Microstructure of Mats in Iron-Depositing Hot Springs. *FEMS Microbiol. Ecol.* **2000**, *32* (3), 181–196.

43 Stal, L. J. Physiological Ecology of Cyanobacteria in Microbial Mats and Other Communities. *New Phytologist* **1995**, *131* (1), 1–32.

44 Prieto-Barajas, C. M.; Valencia-Cantero, E.; Santoyo, G. Microbial Mat Ecosystems: Structure Types, Functional Diversity, and Biotechnological Application. *Electron. J. Biotechnol.* **2018**, *31*, 48–56.

45 Paerl, H. W.; Pinckney, J. L.; Steppe, T. F. Cyanobacterial-Bacterial Mat Consortia: Examining the Functional Unit of Microbial Survival and Growth in Extreme Environments. *Environ. Microbiol.* **2000**, *2* (1), 11–26.

46 Hann, M. Factors Impacting the Cultivation, Structure, and Oxygen Profiles of Oxygenic Photogranules for Aeration-Free Wastewater Treatment. EWRE Masters Projects, UMass Amherst **2018**.

Progression in photogranules and its effect on oxygenic function for aeration-free wastewater treatment

Ahmed S. Abouhend,[†] Kim Milferstedt,[‡] Jérôme Hamelin,[‡] Abeera A. Ansari,[†] Caitlyn Butler,[†] Blanca I. Carbajal-González,[§] Chul Park[*,†]

[†]Department of Civil and Environmental Engineering, University of Massachusetts Amherst, Amherst, Massachusetts 01003, United States
[‡]LBE, Univ Montpellier, INRA, Narbonne F-11100, France
[§]Science Center Microscopy Facility, Mount Holyoke College, South Hadley, Massachusetts 01075, United States
[1]Corresponding author: chulp@umass.edu

Detailed Materials and Methods for:

Source of photogranular biomass. Photogranular biomass investigated in this study was collected from laboratory-scale reactors which were seeded with hydrostatically formed photogranules and operated in sequencing batch mode to treat primary-effluent wastewater without aeration.[17] Reactors were operated under light-dark cycles for five months. Light conditions were provided by fluorescent-light bulbs at an approximately photosynthetically active radiation (PAR) of 150 μmol/m^2-s on the reactor surface. The reactors were mixed at approximately 100 rpm using overhead stirrers equipped with a stainless-steel impeller. Mixing conditions in reactors created an average velocity gradient (G) of 40 1/s and Kolmogorov microscale (η) of 160 μm. Reactors were operated at a hydraulic retention time (HRT) of 0.75–0.9 d and an average solids retention time (SRT) of 30 d. The photogranular biomass was collected from the reactors during the steady-state period. During this period, the size of photogranules was in the range of 0.1–4.5 mm in diameter. Detailed reactor operation and system performance are shown in Abouhend *et al.*[17]

Size separation of photogranular biomass. The photogranular biomass was classified based on size according to the wet-sieving method to achieve an adequate degree of separation between the individual photogranules.[28] Briefly, a 500 mL of mixed biomass was collected from reactors and suspended in a glass beaker containing the reactor's effluent to a total volume of 4 L. The biomass in effluent was then passed through certified testing sieves (Gilson, V200CH) with opening diameters of 0.2 mm, 0.5 mm, 1 mm, 1.7 mm, 2.5 mm, 3.5 mm, and 4.5 mm. The following size classes were obtained: 1) <0.2 mm; 2) 0.2–0.5 mm; 3) 0.5–1 mm; 4) 1–1.7 mm; 5) 1.7–2.5 mm; 6) 2.5–3.5 mm; and 7) 3.5–4.5 mm. The OPG biomass captured on each sieve was washed three times and transferred into a glass beaker containing reactor effluent with a total volume of 500 mL. To ensure accurate size classification, digital images for each size class in Petri dishes were collected and subjected to particle size analysis using the software ImageJ.[35] Particle size analysis confirmed the accurate size separation.

Microscopy. Brightfield, fluorescence, and scanning electron microscopy (SEM) were performed on individual photogranules in the size range of 0.1–4.5 mm to investigate the structure of the photogranules produced during reactor operation.

Brightfield and fluorescence microscopy were done following the procedure presented in Milferstedt *et al.*[10] Cross sections of photogranules were created as follows: 1) the entire photogranule was fixed in Tissue-Tek OCT Compound 4583 (Sakura Finetek, USA); 2) the photogranule was then frozen

at −80 °C; 3) the photogranule was removed from the freezer and sectioned at the maximum diameter under a Leica stereomicroscope using a scalpel; and 4) the obtained sectioned photogranules were immediately imaged. The thickness of the cyanobacterial layer and the diameter of non-cyanobacterial core biomass in photogranules were determined from the light and phycocyanin autofluorescence images of cross-sectioned photogranules using the software ImageJ.[35] The volume of non-cyanobacterial core biomass was directly calculated from its diameter using an Excel spreadsheet.

Photogranules for SEM were prepared following the procedure presented in Milferstedt *et al.*[10] Briefly, the entire photogranule was suspended in an unbuffered glutaraldehyde solution (1%) and gently shaken. After 3–4 h, photogranules were picked from solution and cross-sectioned on wax paper at the maximum diameter under a stereomicroscope. Photogranules and cross-sectioned photogranules were then rinsed with phosphate buffer solution (50 mM $Na_2HPO_4 \cdot 2H_2O$; 50 mM $NaH_2PO_4 \cdot H_2O$; pH = 7) three times over 30 min (10 min each). Next, samples were resuspended in osmium tetroxide solution (1%), agitated for 1.5 h at room temperature, and then rinsed again with phosphate buffer for 15 min. Samples were washed with Milli-Q water three times over 40 min. For dehydration, samples were suspended in a graded ethanol series (25%, 50%, 75% and 100%) for 20 min in each grade. The samples were then dried using tertiary butanol method.[29] Lastly, photogranule samples were sputter-coated with 1-2 nm gold-palladium using a Polaron E5100 sputter coater. SEM images were taken using a FEI Quanta 200 SEM operated at 15 kV.

Measurements of chlorophylls in photogranules. Three 10 mL biomass samples were transferred in 50 mL screw-cap centrifuge tubes and then centrifuged at 12,000 rpm for 10 min at 4°C to separate photogranules from liquid. For chlorophyll extraction, liquid was removed, and the photogranule pellet was resuspended in aqueous acetone solution [one-part saturated magnesium carbonate solution (1%) in nine-parts of acetone] to a volume of 10 mL. Samples were then homogenized at 700 rpm for 30 s and incubated overnight at 4 °C. Chlorophyll *a*, *b* and *c* concentrations (mg/mL) in the final extracts were determined spectrophotometrically following Standard Methods (10200H).[30] Next, the weight fraction of chlorophyll *a*, *b*, and *c* in each photogranule size class was obtained by dividing chlorophyll concentration (mg/L) by volatile suspended solids (VSS) concentration (mg/L) and then multiplying by 100. Chlorophyll measurements were done on triplicate biomass samples.

Measurement of phycobilin in photogranules. The methods by Bennett and Bogorad[31] and Islam *et al.*[32] were modified and used to determine phycobiliprotein content in photogranule samples. Briefly, three 10 mL biomass samples were pipetted in 50 mL centrifuge tubes, and centrifuged at 12,000 rpm for 10 min at 4 °C. The supernatant was discarded, and the biomass pellet was resuspended in 0.025 M phosphate buffer saline solution (pH 7) to a volume of 10 mL. Biomass samples in phosphate buffer saline solution were then homogenized at 700 rpm for 1 min. After homogenization, samples were sonicated at 20% strength for 2 min, and then centrifuged at 12,000 rpm for 10 min. The absorbance of supernatant was measured spectrophotometrically at the wavelengths 562, 615 and 652 nm. The equations by Bennett and Bogorad[31] were used to quantify the phycocyanin (PC), phycoerythrin (PE) and allophycocyanin (APC). Total phycobilin concentration (mg/mL) in samples was calculated as the sum of PC, PE and APC concentrations. Finally, the weight fraction of phycobilin in each photogranule size class was obtained by dividing phycobilin concentration (mg/L) by volatile suspended solids (VSS) concentration (mg/L) and then multiplying by 100.

Extracellular polymeric substances (EPS) in photogranules. EPS was extracted from the photogranular biomass following the sequential sonication and base extraction method presented in Ansari *et al.*[18] Three 10 mL biomass samples were pipetted into 50 mL centrifuge tubes and centrifuged at 12,000 rpm

for 10 min at 4 °C. The supernatant was then removed, and the biomass pellet was resuspended in 10 mL phosphate buffer saline (PBS) solution (10 mM NaCl, 1.2 mM KH_2PO_4, and 6 mM Na_2HPO_4). Samples were then homogenized at 700 rpm for 30 s. Homogenization was followed by sonication at 10% strength for 40 s, and then centrifugation at 12000 rpm for 10 min. After centrifugation, the supernatant was collected and filtered with 0.45 μm cellulose filter. This supernatant was considered as the "biomass-bound EPS extracted by sonication". The remaining biomass pellets after sonication extraction were resuspended in 10 mL PBS solution. The pH of samples was adjusted to 10.5 using 1 M NaOH. The samples were then shaken at 400 rpm for 2 h at 4 °C. Next, samples were centrifuged at 12000 rpm for 10 min. The supernatant was filtered with a 0.45 μm cellulose filter. This supernatant was considered as the "biomass-bound EPS extracted by base" The total biomass-bound EPS was calculated by taking the sum of biomass-bound EPS extracted by sonication and base. EPS samples were either processed or frozen at −20 °C until the analysis. Polysaccharide and protein concentrations in extracted EPS were measured using Dubois method[33] and modified Lowry method,[34] respectively. Finally, EPS protein and polysaccharide content of each photogranule size class (mg/g VSS) was obtained by dividing EPS protein and polysaccharides concentration (mg/L) by volatile suspended solids (VSS) concentration (g/L).

Specific oxygen production rate (SOPR) of photogranules. The oxygen production rate (mg O_2/L-h) of each photogranule size class was determined in a closed batch system following the procedure shown in Abouhend et al.[17] Briefly, each photogranule size class was suspended in 2x diluted primary-effluent wastewater and then transferred to a 300 mL biochemical oxygen demand (BOD) bottle with no headspace. The BOD bottles were purged with nitrogen, mixed at 100 rpm using a magnetic stirrer, and then exposed to light at photosynthetically available radiation (PAR) of approximately 150 μmol/m^2-s. The dissolved oxygen concentration in the BOD bottles was monitored over time until dissolved oxygen gets saturated. We plotted the dissolved oxygen concentration versus time and then determined "the net oxygen production rate (OPR_{net})" of photogranular biomass as the slope of the linear-regression line.

    We also measured the initial and final concentrations of COD and nitrogen species in the liquid phase. Next, we calculated the theoretical amount of oxygen consumed ($OPR_{consumed}$) for organic matter and ammonia oxidation during the batch reaction which was determined based on the equivalent amounts of oxygen consumed for organic matter oxidation and nitrification over time. The total OPR (OPR_{total}) of the OPG biomass was obtained by taking the sum of OPR_{net} and $OPR_{consumed}$. The specific OPR (SOPR) of photogranular biomass (mg O_2/g VSS-h) was then obtained by dividing OPR_{total} of each size group by the concentration of VSS used in the batch reaction. The oxygen production experiment was conducted in triplicate.

Analytical methods. Measurements of total and volatile suspended solids of the photogranule size classes were conducted according to Standard Methods 2540D/E.[30] Chemical oxygen demand (COD) was determined following Standard Methods 5220D.[30] Nitrogen species (ammonia, nitrite, and nitrate) were measured using ion chromatography (Metrohm 830). Zone settling velocity (ZSV) and sludge volume index (SVI) of photogranule size classes were determined following Standard Methods (2710D/E).[30] The roundness of photogranules was determined using the software ImageJ.[35] Roundness values were obtained in the range of 0–1. A perfect granule had a roundness of 1 while a needle-shaped particle had a roundness close to 0.

Statistical analysis. The two-samples *t-test* was performed to determine whether there is a statistically significant difference between the variables. We set the default alpha (α) value at 0.05 so if the p-value is less than 0.05 there is a statistically significant difference between the variables. Regression analysis was also conducted to examine the relationship between the variables.
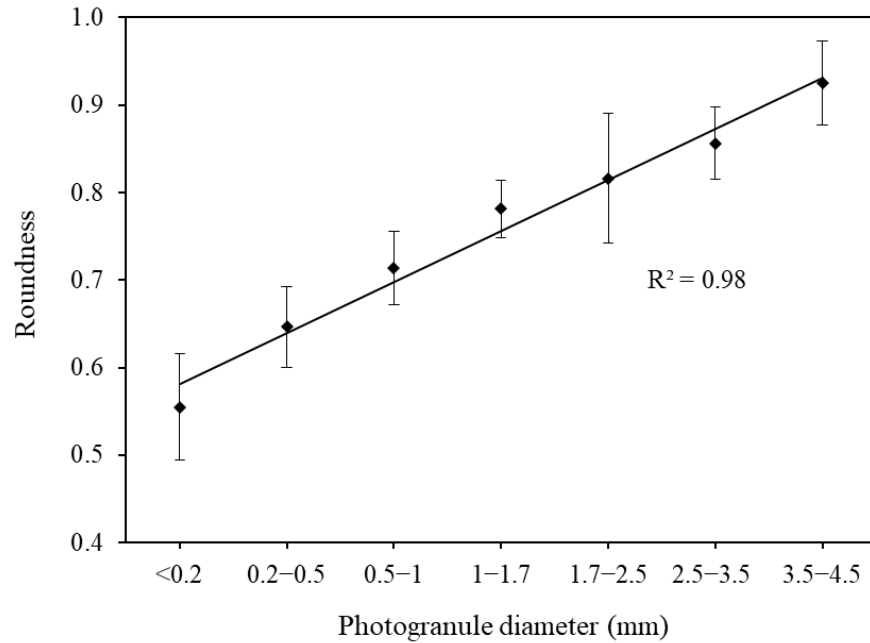
Figure S1. Roundness of photogranules in different size classes. Error bars represent the standard deviation of the roundness of at least 100 photogranules in each size class.
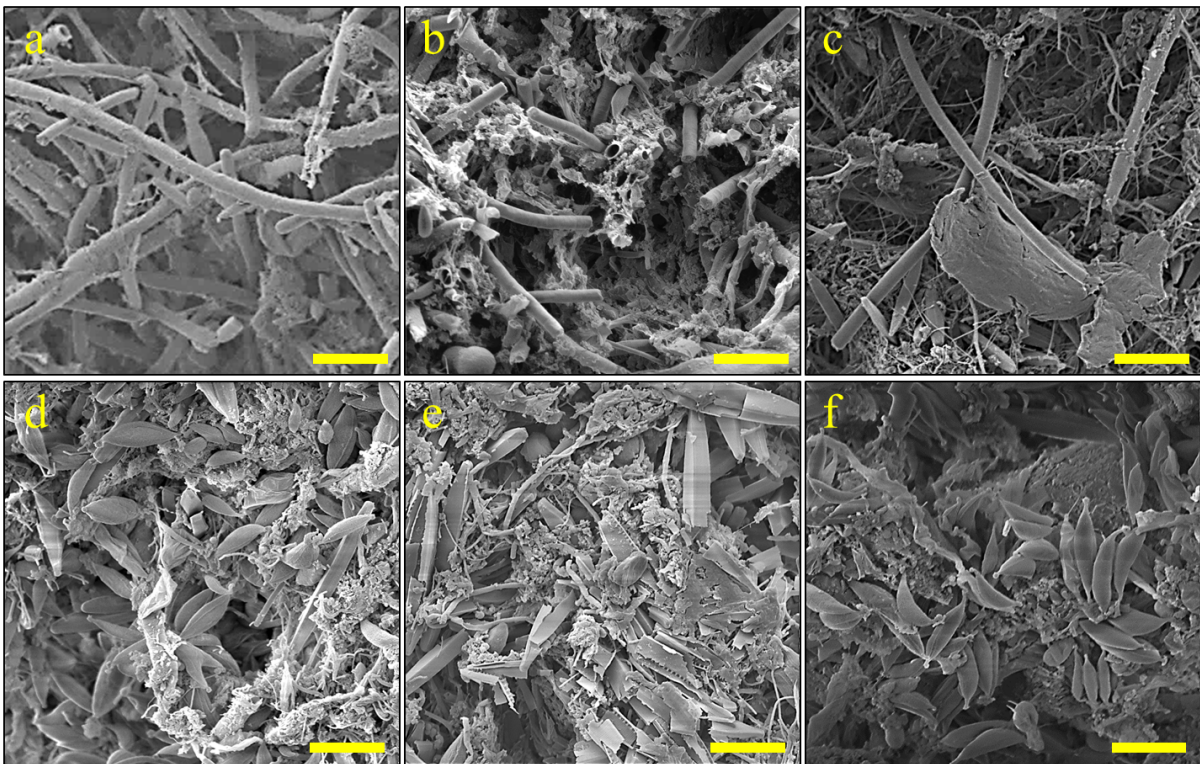

Figure S2. Scanning electron *microscopy* (SEM) of the center of cross-sectioned photogranules in different sizes. (A–C) The center of photogranules smaller than 3 mm in diameter. (D–F) The center of photogranules larger than 3 mm in diameter. Scale bar for all panels is 20 μm.

a

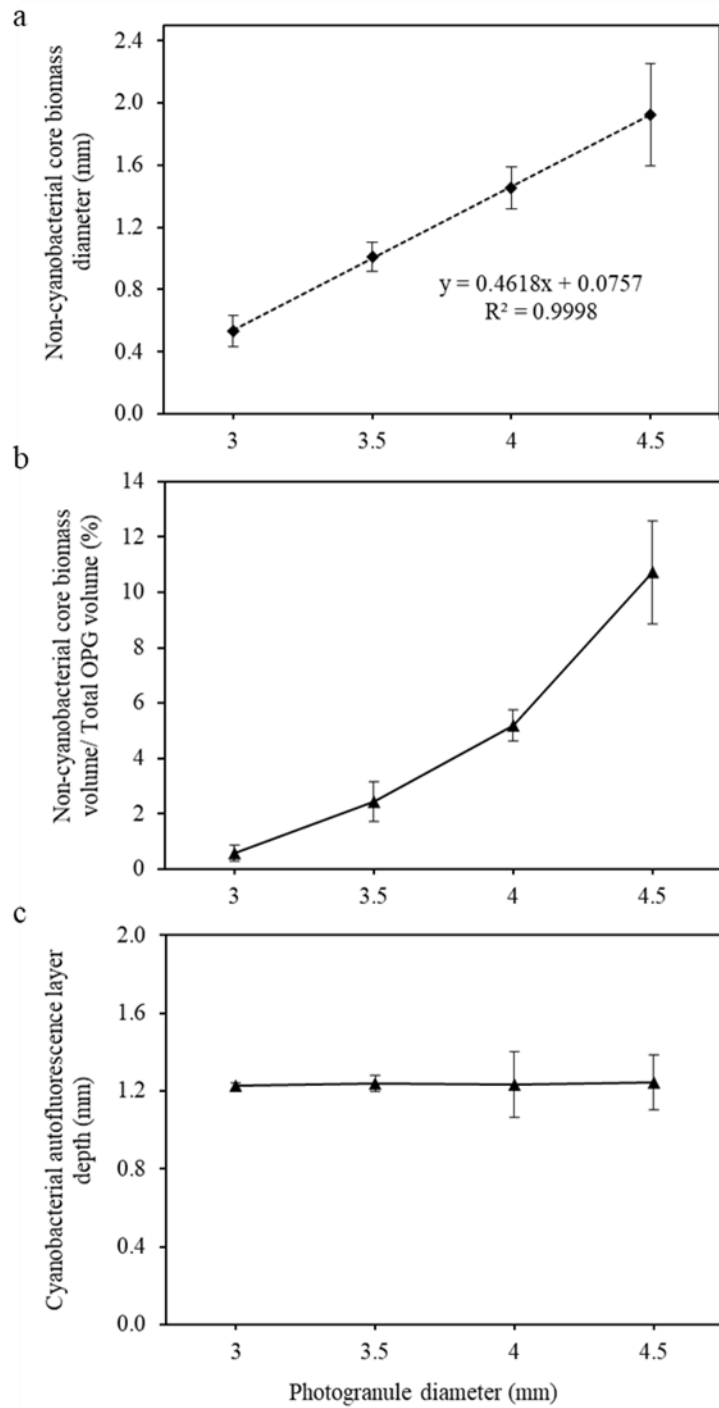$y = 0.4618x + 0.0757$
$R^2 = 0.9998$

b

c

Figure S3. Changes in depth and size of cyanobacterial and non-cyanobacterial biomass in photogranules greater than 3 mm in diameter. (A) Changes in the diameter of non-cyanobacterial core biomass per the diameter of photogranules. (B) Changes in the volume of non-cyanobacterial core biomass in photogranules per the diameter of photogranules. (C) Constant depth of cyanobacterial layer in photogranules greater than 3 mm in diameter. Error bars represent the standard deviations of triplicate measurements.
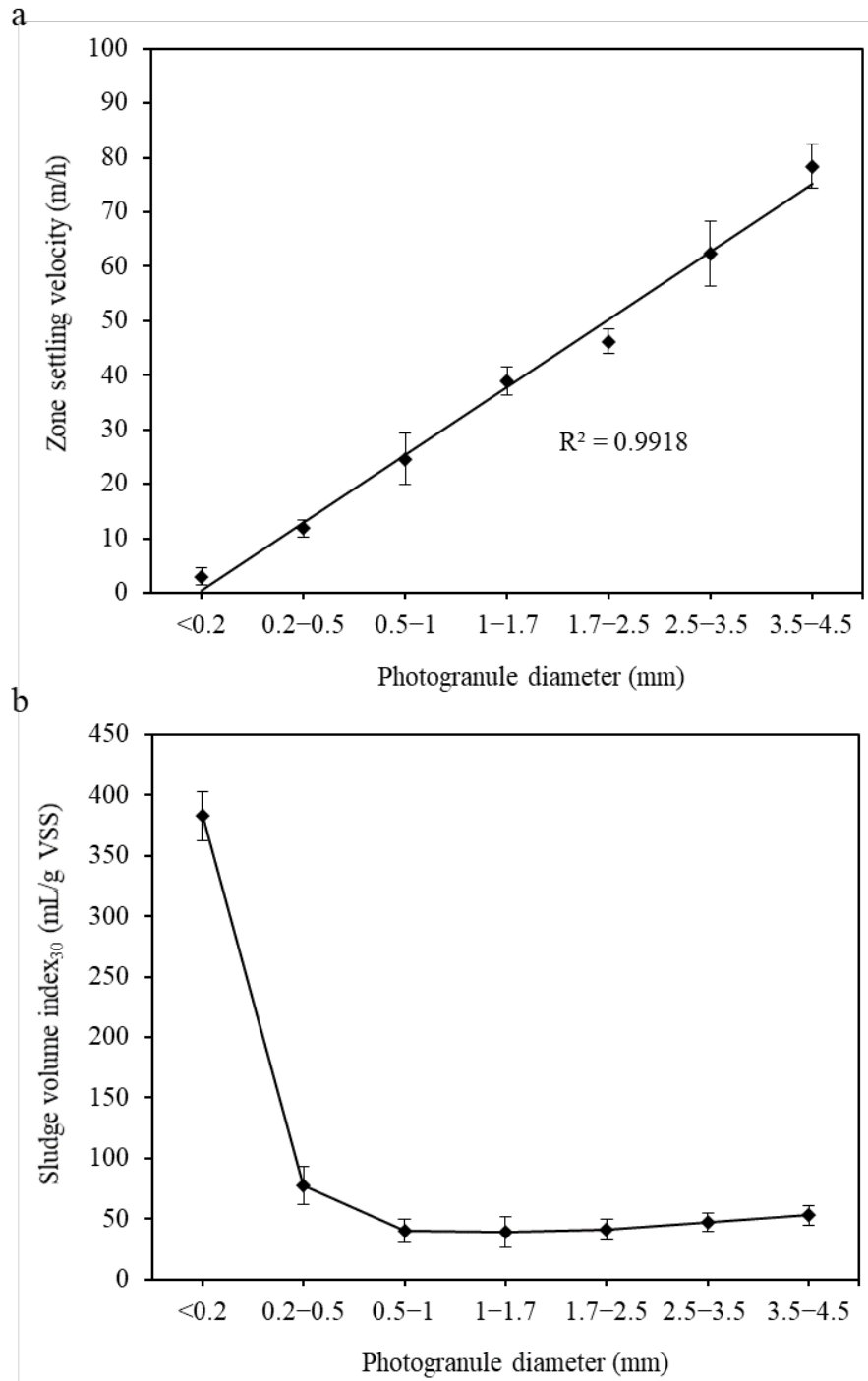
a

b

Figure S4. Settling properties of photogranule in different size classes. (A) Zone settling velocity (ZSV). (B) Sludge volume index (SVI). Error bars represent the standard deviations of triplicate samples.

6